*Kovove Mater. 59 2021 367–377*
*DOI: 10.4149/km_2021_6_367*



# Effect of heat treatment on microstructure and thermal expansion properties of as-cast $(Al_{63}Cu_{25}Fe_{12})_{99}Ce_1$ alloy

Juan Wang, Zhong Yang*, Hongbo Duan, Zhijun Ma, Dong Tao, Jianping Li

*School of Materials and Chemical Engineering, Xi'an Technological University, Xi'an 710021, P. R. China*

Received 17 September 2021, received in revised form 17 October 2021, accepted 19 October 2021

**Abstract**

The heat treatment of $(Al_{63}Cu_{25}Fe_{12})_{99}Ce_1$ alloy was performed at 650, 750, and 850 °C for different holding times. The effects of the heat treatment process on the alloy's microstructure and thermal expansion properties were studied. Results revealed that the cast alloy contained $\beta$-$Al_{0.5}Fe_{0.5}$ phase ($\beta$-phase), $Al_2Cu_3$ phase, $Al_{13}Ce_2Cu_{13}$ phase, and icosahedral quasicrystal I-phase (I-phase). After holding at 750 °C for 6 h, the alloy contains only an I-phase and a small amount of $Al_{13}Ce_2Cu_{13}$ phase. When the heat treatment temperature continued to increase, the I-phase was partially decomposed. After heat treatment, the thermal expansion coefficient of the alloy decreased obviously. Compared with as cast, the thermal expansion coefficient of the alloy decreased by about 10 % after holding at 750 °C for 6 h. The results show that the Al-Cu-Fe-Ce alloy with excellent microstructure and properties can be obtained by an appropriate heat treatment process.

K e y w o r d s: heat treatment, quasicrystal I-phase, microstructure, coefficient of thermal expansion

## 1. Introduction

Quasicrystal materials have attracted much attention because of their good properties [1], such as high hardness [2, 3], wear resistance [4], corrosion resistance [5], etc. So far, common quasicrystal materials mainly include aluminum matrix, magnesium matrix, and titanium matrix. Most of them are metastable quasicrystals, and only a few quasicrystals are thermodynamically stable, such as Al-Cu-Fe quasicrystals. The advantage of Al-Cu-Fe quasicrystal is that aluminum, copper, and iron are three common metal elements. These elements are cheap and non-toxic, which is very suitable for wide application in industry.

Therefore, the discovery of Al-Cu-Fe quasicrystals by Tsai et al. [6] has attracted extensive attention. This quasicrystal material has a new and highly complete structure and is very stable in thermodynamics [7, 8]. Generally, stable quasicrystal materials can be prepared by the conventional casting method, but there are few quasicrystal phases in Al-Cu-Fe quasicrystal alloys prepared by this method. Therefore, a single quasicrystal alloy can be directly prepared from an alloy with quasicrystal composition only when a great solidification rate is adopted, but it is difficult to achieve a great solidification rate in actual production. However, when the solidification rate is slow, a basic single quasicrystal alloy can be obtained through an appropriate heat treatment [9–11].

According to the relevant literature [12–14], the heat treatment process often involves phase transformation. G. Rosas et al. studied the transformation process of various phases in different alloys close to the ternary composition value after holding at 600, 700, and 800 °C for different times [14]. The results show that for $Al_{58}Cu_{28}Fe_4$ alloy, after heat treatment at 700 °C, the quasicrystal phase changes to all $\beta$-phase, and $Al_{68}Cu_{27}Fe_5$ alloy is transformed into w-$Al_7Cu_2Fe$ after heat treatment at 700 °C. It shows that the composition of the alloy and different heat treatment temperatures greatly influence the phase composition after transformation. According to Lilong Zhu's research [15], for $Al_{63}Cu_{25}Fe_{12}$ alloy, the I-phase exists stably at 700 and 800 °C.

At the same time, according to our previous research [16], when preparing quasicrystal alloy by con-

*Corresponding author: e-mail address: yz750925@163.com

ventional casting method, adding Ce known as industrial vitamin on the basis of $Al_{63}Cu_{25}Fe_{12}$ alloy can increase the formation of I-phase to a certain extent. Especially when the content of Ce in the alloy is 1 at.%, the content of the I-phase in the alloy is higher. To further improve the content of the I-phase in the alloy, the $(Al_{63}Cu_{25}Fe_{12})_{99}Ce_1$ alloy was heat-treated at different heating temperatures and holding times to further increase the content of I-phase in the alloy, and the role of Ce in the heat treatment process was discussed.

This paper studies the microstructure and properties of $(Al_{63}Cu_{25}Fe_{12})_{99}Ce_1$ alloy after heat treatment and analyzes the role of Ce in the heat treatment process. The $(Al_{63}Cu_{25}Fe_{12})_{99}Ce_1$ alloy prepared by conventional casting method was heat-treated at different temperatures (650, 750, and 850 ℃ and at different holding times to explore the effect of Ce addition on the microstructure changes of the alloy during heat treatment. The aim was to improve the content and morphology of the I-phase in the alloy at low heat treatment temperatures and obtain quasicrystal alloy with high I-phase content, good thermal expansion performance, and excellent microstructure.

## 2. Experimental details

### 2.1. Preparation of materials

In this study, the following raw materials were used, including high-purity Al (99.99 %), Cu, Al-30Ce (99.5 %, wt.%), and Al-60Fe (99.98 %) master alloys. In brief, each raw material was placed in the copper crucible within the vacuum chamber filled with argon to prevent oxidation. Afterward, the arc was used to melt the materials, followed by the flowing cold water surrounding copper crucible walls to achieve rapid cooling to ambient temperature in 5 min. After that, the resultant sample was subjected to flipping and remelting four times for improving uniformity.

Melted samples were heat-treated in a box resistance furnace. According to the TGA test results of the as-cast $(Al_{63}Cu_{25}Fe_{12})_{99}Ce_1$ alloy and relevant studies [17–19], the heat treatment temperature was set at 650, 750, and 850 ℃, and they were kept at these three temperatures for 3, 5, and 6 h, respectively, and then cooled with the furnace. The heating rate at three temperatures was 10 ℃ $min^{-1}$. As-cast and heat-treated samples were mechanically polished and adopted the diluted Keller's reagent (consisting of 2.5 mL $HNO_3$, 1.0 mL HF, 1.5 mL HCl, and 95 mL water) to be the etchant for those samples to polish.

### 2.2. Characterization of materials

The phase composition of as-cast and heat-treated samples was analyzed by an X-ray diffractometer (XRD-6000). The microstructure of the alloy was characterized by scanning electron microscope, energy spectrum analyzer, and transmission electron microscope (JEM-2010). The proportion of I-phase in as-cast and heat-treated $(Al_{63}Cu_{25}Fe_{12})_{99}Ce_1$ alloy was calculated by Image-Pro Plus 6.0 software. Under the same process, each sample was calculated 30 times according to the scanned images with different magnification, and then the average value was taken as the final calculation result to ensure the accuracy of the experimental data.

Microstructures were analyzed using scanning electron microscopy (SEM, TESCAN, VEGA II-XMU). The SEM instrument was coupled with high-resolution transmission electron microscopy (HRTEM, JM-2010) and energy-dispersive X-ray spectroscopy (EDS). We also conducted EDS point analysis and X-ray elemental mapping for exploring diverse phase nature and elemental distribution of $(Al_{63}Cu_{25}Fe_{12})_{99}Ce_1$ alloy.

In the presence of Cu K$\alpha$ radiation ($\lambda$ = 0.1542 nm), we recorded $(Al_{63}Cu_{25}Fe_{12})_{99}Ce_1$ alloy for its X-ray diffraction (XRD-6000) patterns. The scanning speed and angle were set at 4° $min^{-1}$ and 20°–90°, respectively. Meanwhile, thermal analysis was conducted using high-temperature differential scanning calorimetry (TGA/DSC1). The experiments were conducted under an atmosphere of Ar, and we set the heating rate at 20 ℃ $min^{-1}$. The mass of the sample used for the DSC experiments was approximately 30 mg. Samples were put into alumina crucibles and heated and cooled at 20 ℃ $min^{-1}$ under a pure argon flow.

The thermal expansion characteristics of as-cast and heat-treated $(Al_{63}Cu_{25}Fe_{12})_{99}Ce_1$ alloy were studied by a thermomechanical analyzer (TMA/SDTA-840). The heating temperature was from room temperature to 500 ℃ at the 5 ℃ $min^{-1}$ heating rate, protected by argon atmosphere, and the sample size was ø 5 mm × 5 mm. The computer was utilized to record all data, while Mettler Toledo thermal analysis system was adopted for data analysis.

## 3. Results

### 3.1. DSC analysis of as-cast $(Al_{63}Cu_{25}Fe_{12})_{99}Ce_1$ alloy

Figure 1 shows the DSC curves for heating of the investigated alloy. Combined with relevant literature [20–23], there are four endothermic peaks in $(Al_{63}Cu_{25}Fe_{12})_{99}Ce_1$ alloy, namely, the endothermic peak near 587 ℃ ($Al_2Cu_3$ phase), the endothermic peak near 691.9 ℃ ($Al_{13}Ce_2Cu_{13}$ phase), the endothermic peak near 882 ℃ (I-phase),

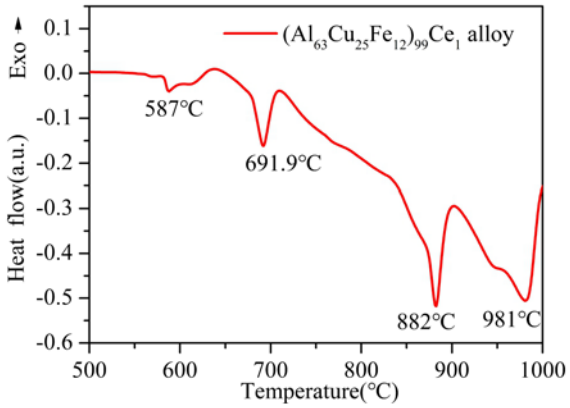


Fig. 1. DSC curves for heating of the examined $(Al_{63}Cu_{25}Fe_{12})_{99}Ce_1$ alloy.

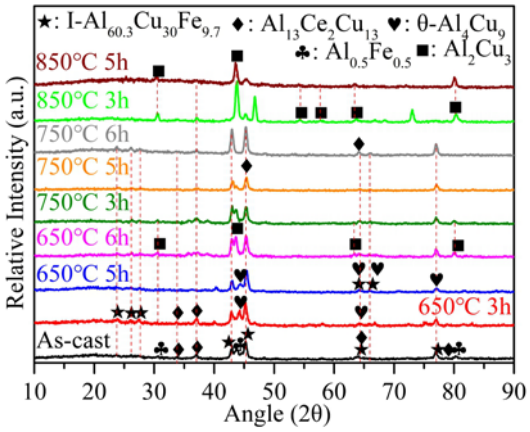


Fig. 2. XRD patterns of $(Al_{63}Cu_{25}Fe_{12})_{99}Ce_1$ alloy in as-cast and heat treating.

and the endothermic peak near 981 ℃ ($\beta$-phase).

The heat treatment temperature was set at 650 ℃, mainly to ensure the melting of the low-temperature $Al_2Cu_3$ phase, and the reactions ($\beta$-phase + AlCu phase → I-phase) occur between $Al_2Cu_3$ phase and $\beta$-phase during heat treatment.

At the same time, to study the stability of the $Al_{13}Ce_2Cu_{13}$ phase, heat treatment was carried out at 750 ℃. The purpose was to study whether the $Al_{13}Ce_2Cu_{13}$ phase existed and whether it would change morphology in the subsequent cooling process when the heat treatment temperature was higher and lower than the melting point of the $Al_{13}Ce_2Cu_{13}$ phase. However, the primary purpose of heat treatment was to improve the formation of the I-phase, so the maximum heat treatment temperature was 850 ℃ to ensure that I-phase would not melt.

### 3.2. X-ray diffraction analysis of $(Al_{63}Cu_{25}Fe_{12})_{99}Ce_1$ alloy in as-cast and heat treating

Figure 2 shows the XRD patterns of $(Al_{63}Cu_{25}Fe_{12})_{99}Ce_1$ alloy in as-cast and heat treating. As-cast, the $(Al_{63}Cu_{25}Fe_{12})_{99}Ce_1$ alloy is mainly composed of four phases: a $\beta$-$Al_{0.5}Fe_{0.5}$ phase ($\beta$-phase), an $Al_2Cu_3$ phase, an $Al_{13}Ce_2Cu_{13}$ phase, and an I-$Al_{60.3}Cu_{30}Fe_{9.7}$ phase (I-phase). With a cubic crystal system, the $\beta$-$Al_{0.5}Fe_{0.5}$ phase ($\beta$-phase) crystallizes in the Pm-3m space group, and its lattice parameter is $a = 0.291$ nm. The $Al_2Cu_3$ phase crystallizes in the P63/mmc space group with a hexagonal crystal system, and its lattice parameters are $a = 0.829$ nm, $b = 0.829$ nm, and $c = 0.497$ nm. The Al13Ce2Cu13 phase crystallizes in the Fm-3c space group with a cubic crystal system, and its lattice parameters are $a = 1.189$ nm, $\alpha = 90°$. The fourth type of phase is the I-$Al_{60.3}Cu_{30}Fe_{9.7}$ phase (I-phase) with an icosahedral construction.

When the alloy was heat-treated at different temperatures, the constituent phases in the alloy changed. When the heating temperature increased from 650 to 750 ℃, the diffraction peak intensity corresponding to I-phase in the alloy increased. The heating temperature continued to rise to 850 ℃, and the I-phase decomposed instability. It shows that the heating temperature of 750 ℃ is most suitable for the transformation from other phases to I-phase. At the same time, the Al13Ce2Cu13 phase always exists with increasing heating temperature, indicating that this phase is stable.

At 750 ℃, the peak strength of the I-phase and other phases changed with the increase of holding time. With the increasing holding time, the diffraction peak intensity corresponding to the I-phase increased, and that of the $\beta$-phase decreased. It shows that I-phase is stable at this temperature, and the $\beta$-phase tends to disappear gradually. After holding at 750 ℃ for 6 hours, the alloy contained only the I-phase and part of the $Al_{13}Ce_2Cu_{13}$ phase.

Phase transformation occurred during heat treatment because the cooling speed was slow in preparing as-cast alloy. There are not only $\beta$-phase with a melting point higher than I-phase, AlCu phase with a melting point lower than I-phase, and a small number of other phases in the alloy. In the subsequent heat treatment process, the melting of these low melting point phases (such as the AlCu phase with high copper content) promoted the transformation of the I-phase.

### 3.3. Microstructural characterization of $(Al_{63}Cu_{25}Fe_{12})_{99}Ce_1$ alloy

Figure 3 shows the SEM micrographs of the as-cast $(Al_{63}Cu_{25}Fe_{12})_{99}Ce_1$ alloy. Figures 3a, b are the low magnification and high magnification scanning morphologies of the alloy.

Table 1. Compositional analysis of different phases in the $(Al_{63}Cu_{25}Fe_{12})_{99}Ce_1$ alloy (at.%)

| Alloy | Location | Composition | | | | Possible phases |
|---|---|---|---|---|---|---|
| | | Al | Fe | Cu | Ce | |
| $(Al_{63}Cu_{25}Fe_{12})_{99}Ce_1$ | Black (A) | 70.46 | 23.88 | 5.66 | – | $\beta$-$Al_{0.5}Fe_{0.5}$ |
| | Black grey (B) | 62.08 | 12.2 | 25.72 | – | I-phase |
| | Light grey (C) | 52.57 | 4.69 | 42.74 | – | $Al_2Cu_3$ |
| | White (D) | 42.54 | 2.16 | 47.99 | 7.31 | $Al_{13}Ce_2Cu_{13}$ |

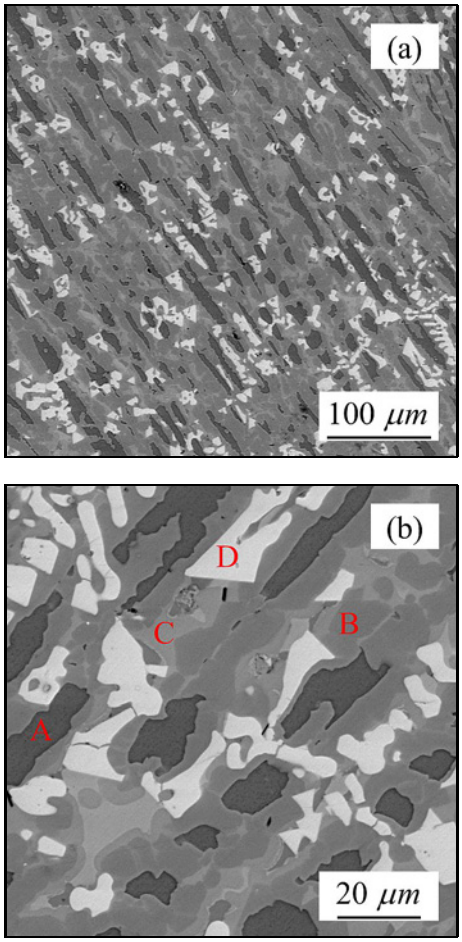


Fig. 3. SEM micrographs of the as-cast $(Al_{63}Cu_{25}Fe_{12})_{99}Ce_1$ alloy: (a) and (b) are the low magnification and high magnification scanning morphologies of the alloy of the as-cast $(Al_{63}Cu_{25}Fe_{12})_{99}Ce_1$ alloy, respectively.

The microstructure of the $(Al_{63}Cu_{25}Fe_{12})_{99}Ce_1$ alloy is composed of four areas: dark (A), dark grey (B), light grey (C), and white (D). EDS was conducted in the representative areas to identify the nature of these areas, and the energy spectrum analysis is shown in Table 1. Meanwhile, combined with the previous XRD analysis results, we know that these four regions represent four different phases, a $\beta$-phase, an I-phase, an $Al_{13}Ce_2Cu_{13}$ phase, and an $Al_2Cu_3$ phase. Table 1 summarizes the chemical composition of each phase shown in $(Al_{63}Cu_{25}Fe_{12})_{99}Ce_1$ alloy. The dark area (A) in the SEM image with a small amount of copper (5.66 at.% in EDS) thus corresponds to the $\beta$-phase. The black grey area (B) represents the I-phase. The white area (D) represents the $Al_{13}Ce_2Cu_{13}$ phase with a small amount of iron (2.16 at.% in EDS). The remaining light grey area (C) matches with the $Al_2Cu_3$ phase.

The cooling rate of quasicrystal alloy prepared by the conventional casting method was slow, and the solidification process of the ingot was as follows: At the beginning of solidification, $\beta$-phase was directly precipitated from the liquid phase in dendritic distribution and became the first precipitated phase. With the decrease of temperature, a peritectic reaction occurred between $\beta$-phase and some liquid phases generated the I-phase ($L + \beta \rightarrow I$), and the remaining liquid phase solidified into the $Al_2Cu_3$ phase and $Al_{13}Ce_2Cu_{13}$ phase. At the same time, the addition of Ce caused component undercooling [24], which refined the constituent phases in the alloy to a certain extent. After heat treatment at 750 ℃ for 6 h, the $(Al_{63}Cu_{25}Fe_{12})_{99}Ce_1$ alloy contained only an I-phase and a small amount of $Al_{13}Ce_2Cu_{13}$ phase.

Combined with the scanning morphology of the alloy under each heat treatment process (as shown in Figs. 4, 5), the microstructure transformation during heat treatment was analyzed.

Figures 4a–c show the microstructure of $(Al_{63}Cu_{25}Fe_{12})_{99}Ce_1$ alloy after heat treatment at 650 ℃ for 3, 5, and 6 h, respectively. After holding at 650 ℃ for 3 h, there was a part of the AlCu phase, and $\beta$-phase reacted to form I-phase, but some AlCu phase was still retained due to low heating temperature, short holding time, and insufficient atomic diffusion. When the holding time was increased to 5 h at 650 ℃, the microstructure of $\beta$-phase changed from strip to ball and then gradually dissolved in the subsequent holding process.

Figures 5a–c show the microstructure of $(Al_{63}Cu_{25}Fe_{12})_{99}Ce_1$ alloy after holding at 750 ℃ for 3, 5, and 6 h, respectively. After holding at 750 ℃ for 3 h, the AlCu phase in the alloy was consumed entirely, leaving only $\beta$-phase, I-phase, and white $Al_{13}Ce_2Cu_{13}$ phase. With the extension of holding time, the $\beta$-phase gradually spheroidized and completely dissolved.

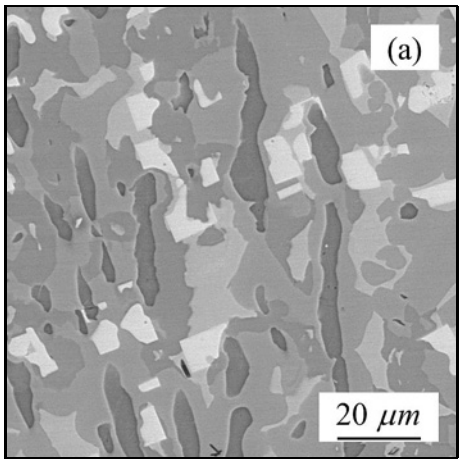


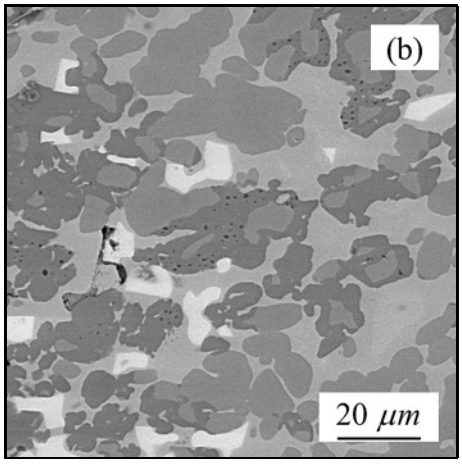


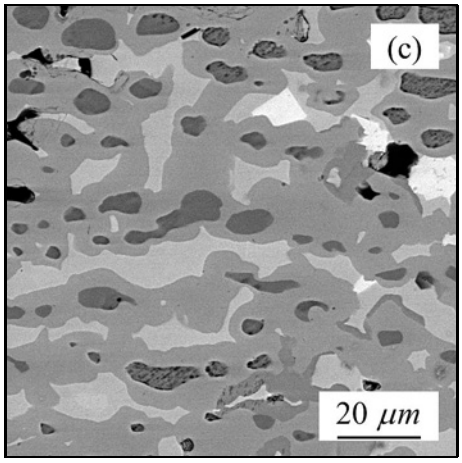


Fig. 4. Microstructure of $(Al_{63}Cu_{25}Fe_{12})_{99}Ce_1$ alloy after heat treatment at 650 °C for (a) 3 h, (b) 5 h, and (c) 6 h.

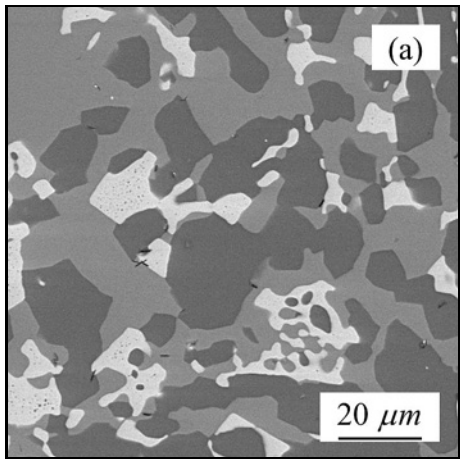


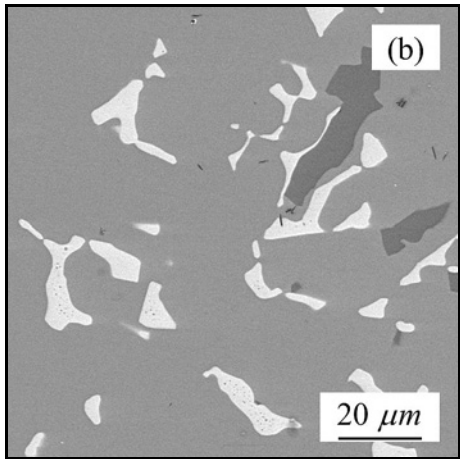


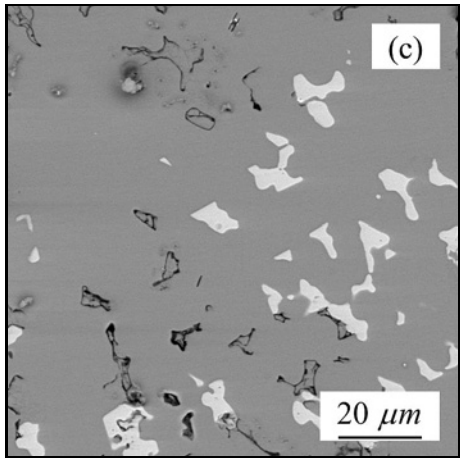


Fig. 5. Microstructure of $(Al_{63}Cu_{25}Fe_{12})_{99}Ce_1$ alloy after heat treatment at 750 °C for (a) 3 h, (b) 5 h, and (c) 6 h.

As shown in Fig. 5a–c, when the heating temperature was 750 °C, the holding time increased, the $\beta$-phase in the black area decreased significantly, and the I-phase in the gray area increased significantly. It shows that $(Al_{63}Cu_{25}Fe_{12})_{99}Ce_1$ alloy has a gradual transformation from $\beta$-phase to I-phase during heating. With the extension of holding time, the $\beta$-phase in the black region gradually disappeared, and there are only I-phase and part of the $Al_{13}Ce_2Cu_{13}$ phase in the alloy. $Al_{13}Ce_2Cu_{13}$ phase always exists in the white region, indicating that this phase has high thermal stability.

The formation of the I-phase was accompanied by the formation of other phases and a non-equilibrium

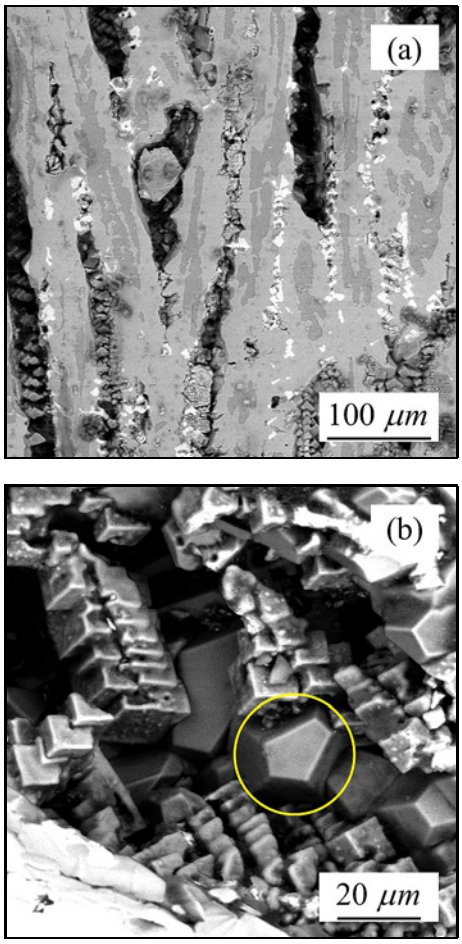


Fig. 6. The low magnification morphology of $(Al_{63}Cu_{25}Fe_{12})_{99}Ce_1$ alloy at 750 °C for 3 h (a); the high magnification scanning morphology of $(Al_{63}Cu_{25}Fe_{12})_{99}Ce_1$ alloy and the locally enlarged view of I-phase (b).

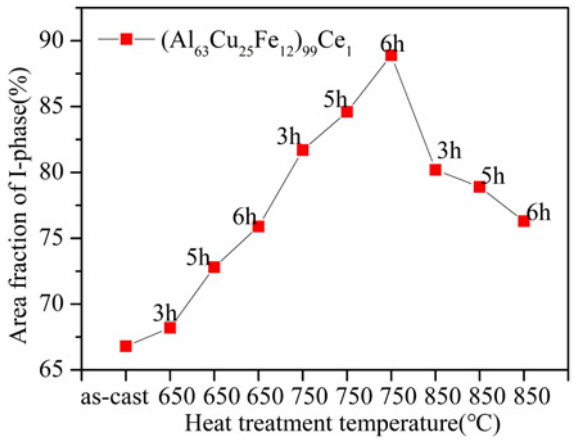


Fig. 7. The proportion of I-phase in as-cast and heat-treated $(Al_{63}Cu_{25}Fe_{12})_{99}Ce_1$ alloy.

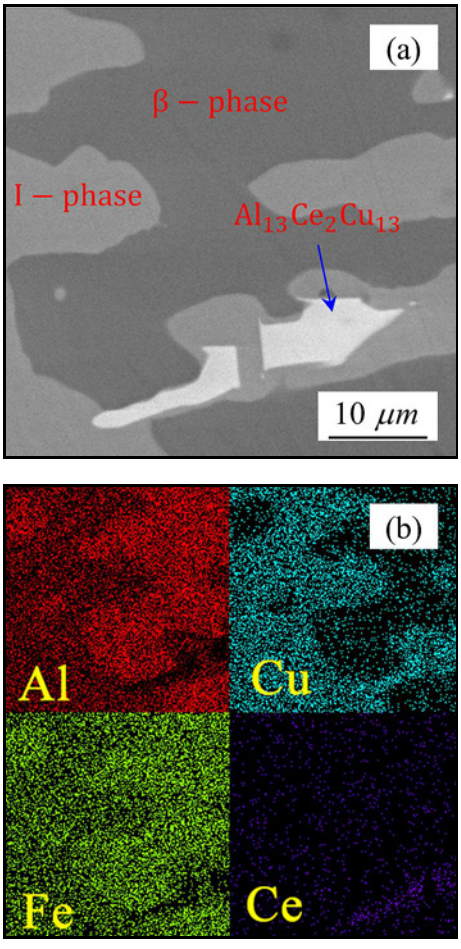


Fig. 8. SEM images (a) and the corresponding element distribution of $(Al_{63}Cu_{25}Fe_{12})_{99}Ce_1$ alloy after 3 h at 750 °C (b).

solidification process. Therefore, there was an uneven phase distribution during the formation of the I-phase in the alloy prepared by the conventional casting method. With the progress of heat treatment, the $\beta$-phase was spheroidized and refined. With the extension of holding time, the $\beta$-phase decreased gradually. In addition, during the heating and insulation process of the $(Al_{63}Cu_{25}Fe_{12})_{99}Ce_1$ alloy, the $\beta$-phase gradually diffused and dissolved, and the distribution was more uniform and fine. It shows that appropriate heating temperature and holding time are not only conducive to the formation of the I-phase but also conducive to a more uniform distribution of microstructure.

The macro morphology of $(Al_{63}Cu_{25}Fe_{12})_{99}Ce_1$ alloy after holding at 750 °C for 3 h was observed and analyzed, as shown in Fig. 6. The alloy contains three phases, which are dark gray areas $\beta$-phase, I-phase in a light gray area, and $Al_{13}Ce_2Cu_{13}$ phase in a white area, and there are a certain number of defects. The reason for the defects is that the appropriate addition of Ce causes component undercooling, increases the

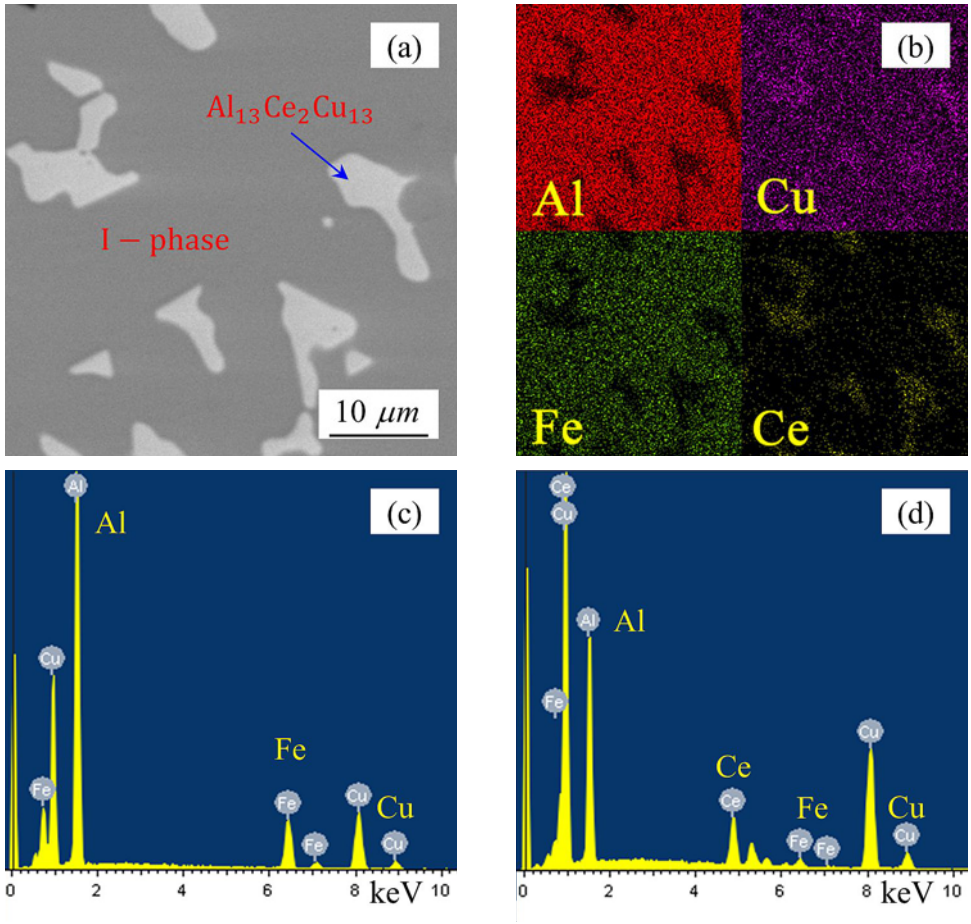


Fig. 9. SEM images and the corresponding element distribution of $(Al_{63}Cu_{25}Fe_{12})_{99}Ce_1$ alloy at 750 ℃ for 6 h (a), (b) and (c), (d) EDS of the I-phase and $Al_{13}Ce_2Cu_{13}$ phase.

undercooling degree in the solidification process of the alloy, and plays the role of refining grains. However, I-phase is a brittle phase; even if it is small and evenly distributed, cracks can not be avoided. At the same time, the microstructure at the defect was observed by high magnification scanning morphologies, and the results are shown in Fig. 6b. The results show that the regions of these defects are typical regular pentagonal I-phase, which further shows that the intrinsic brittleness of the I-phase leads to the generation of defects in the alloy.

Meanwhile, the area proportions of the I-phase formed by $(Al_{63}Cu_{25}Fe_{12})_{99}Ce_1$ alloy after heat preservation at different temperatures were calculated by Image-pro Plus software. The statistical results are shown in Fig. 7. It can be seen from Fig. 7 that the content of the I-phase in as-cast is 66.7 %. With the heating temperature from 650 to 750 ℃, the I-phase gradually increases. However, the proportion of the I-phase decreases with the extension of holding time. The reason is that the I-phase was partially decomposed during heat treatment with the increase of temperature.

The cooling rate of $(Al_{63}Cu_{25}Fe_{12})_{99}Ce_1$ alloy prepared by conventional casting method was not very fast, but the microstructure distribution after solidification is uneven because the formation process of I-phase is a non-equilibrium solidification process. In the subsequent heat treatment process, with the extension of holding time, the elements diffused gradually, and the distribution of each phase in the alloy is more uniform.

However, there is still more $\beta$-phase in the alloy after holding at 750 ℃ for 3 h. High magnification microstructure observation and element area distribution analysis were carried out on the alloy after holding at 750 ℃ for 3 h, as shown in Fig. 8a. The alloy contains three phases, namely $\beta$-phase, I-phase, and $Al_{13}Ce_2Cu_{13}$ phase. According to the element area distribution, the element distribution of each phase in the alloy is further determined. It can be seen from Fig. 8b that Ce is mainly distributed in the $Al_{13}Ce_2Cu_{13}$ phase, and the copper content in the $\beta$-phase is less.

After $(Al_{63}Cu_{25}Fe_{12})_{99}Ce_1$ alloy was kept at 750 ℃ for 6 h, all $\beta$-phase in the alloy was dissolved, and only I-phase and $Al_{13}Ce_2Cu_{13}$ phase were contained in the alloy. Energy spectrum analysis and element

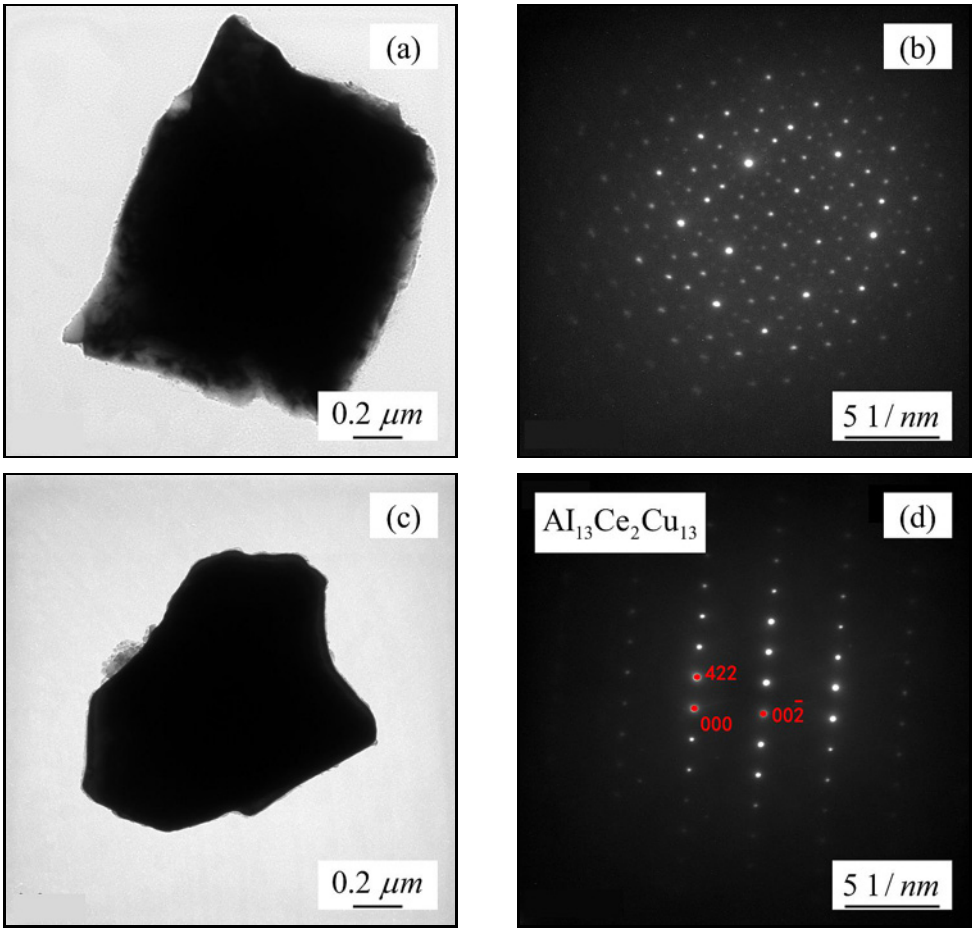


Fig. 10. (a) Microstructure of I-phase in the $(Al_{63}Cu_{25}Fe_{12})_{99}Ce_1$ alloy; (b) selected-area diffraction patterns of the I-phase; (c) microstructure of $Al_{13}Ce_2Cu_{13}$-phase in the $(Al_{63}Cu_{25}Fe_{12})_{99}Ce_1$ alloy; (d) selected-area diffraction patterns of the $Al_{13}Ce_2Cu_{13}$ phase.

area distribution analysis were carried out for each phase in the alloy, as shown in Figs. 9a–d. It can be further seen that most dark gray areas in Fig. 9 are I-phase, and the $Al_{13}Ce_2Cu_{13}$ phase in the white area is evenly distributed.

### 3.4. Transmission electron microscopy of $(Al_{63}Cu_{25}Fe_{12})_{99}Ce_1$ alloy

For a more detailed microstructural characterization, the phase composition of the $(Al_{63}Cu_{25}Fe_{12})_{99}Ce_1$ alloy after heat treatment at 750 ℃ for 6 h was further confirmed by transmission morphology analysis. TEM studies revealed that the specimen consisted of envelope grains, the diameter of which varied from about several hundreds of nanometers to a few microns (Fig. 10a). Moreover, Fig. 10b shows a typical quasicrystal icosahedral electron diffraction pattern. The microstructure and electron diffraction pattern of the $Al_{13}Ce_2Cu_{13}$ phase in the alloy after heat treatment were observed, as shown in Figs. 10c–d, and the phase composition in the alloy was further determined.

### 3.5. Thermal expansion properties of $(Al_{63}Cu_{25}Fe_{12})_{99}Ce_1$ alloy

The thermal expansion coefficient of as-cast $(Al_{63}Cu_{25}Fe_{12})_{99}Ce_1$ alloy under different heat treatment processes was measured, and the results are shown in Fig. 11. The thermal expansion performance of the material is usually characterized by the average linear expansion coefficient, which gives the average value of the sample in a specific temperature range, and its formula is:

$$\alpha = \frac{1}{L_0}\frac{\mathrm{d}L}{\mathrm{d}T}, \tag{1}$$

where $L_0$ is the original size of the sample, $\mathrm{d}L$ is the change of line size of the sample within the corresponding temperature range, $\mathrm{d}T$ is the change of the corresponding temperature, and $\alpha$ is the average linear expansion coefficient.

Figure 11 shows the variation trend of thermal expansion coefficient with the temperature of as-cast $(Al_{63}Cu_{25}Fe_{12})_{99}Ce_1$ alloy and after heat treatment.

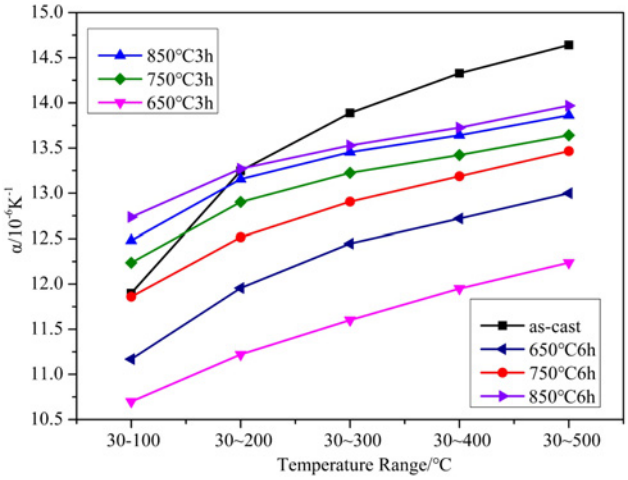


Fig. 11. Variation curve of thermal expansion coefficient of $(Al_{63}Cu_{25}Fe_{12})_{99}Ce_1$ alloy with temperature.

As shown in Fig. 11, with the increase of heating temperature, the thermal expansion coefficient of the alloy in as-cast and various heat treating increases gradually.

When the temperature is low, the expansion coefficient increases rapidly with the increase of temperature, but after 300 ℃, the rise speed of the expansion coefficient slows down with the increase of temperature. This is because the average distance between atoms increases significantly as the temperature increases [25]. After heat treatment, the quasicrystal grains grow and even aggregate, the total grain boundary area decreases, and the blocking effect on dislocation weakens. The resistance to atomic thermal motion decreases, which increases the thermal expansion coefficient of the alloy to a certain extent.

At the same time, with the increase of temperature, the lattice vibration intensifies; that is, the atomic thermal motion energy increases, and the atoms in the lattice are in an unstable state, resulting in the volume expansion of the alloy. Therefore, the expansion coefficient of the alloy increases after heat treatment.

However, the longitudinal comparison shows that the thermal expansion coefficient of the alloy at each temperature stage is almost the largest when it is cast. At the same time, when the alloy is kept at 650 ℃ for 3 and 6 h, the thermal expansion coefficient is small at each temperature stage. The reason is that after heat treatment at 650 ℃, not only does the formation of quasicrystals increase, but also the temperature is low, and the microstructure of the alloy is fine.

When the heating temperature is 750 ℃, the formation of the I-phase further increases. However, the higher heating temperature makes each phase in the alloy tend to coarsen, the total grain boundary area decreases, and the blocking effect on dislocation weakens. Thus, the thermal expansion coefficient of the alloy in each stage is greater than 650 ℃. Compared with the as-cast alloy, when the heating temperature range is 30–500 ℃, the thermal expansion coefficient of the alloy after 6 h at 750 ℃ is about 10 % lower than that of the as-cast alloy under the same conditions. When the heating temperature is 850 ℃, the I-phase is partially decomposed. Moreover, due to the increase of temperature, the microstructure of the alloy is coarse, the total grain boundary area is reduced, and the blocking effect on dislocation is weakened. Thus, the thermal expansion coefficient of the alloy increases further. The experimental results show that the thermal expansion coefficient of the alloy can be significantly reduced by the appropriate heat treatment process and the appropriate addition of Ce.

## 4. Discussion

The process of solid-phase transformation of the as-cast $(Al_{63}Cu_{25}Fe_{12})_{99}Ce_1$ alloy during heat treatment is a process of lattice reorganization or reconstruction completed by atomic diffusion displacement. In other words, the essence of the heat treatment process is the diffusion process of atoms. According to Fick's first law and Fick's second law [26]:

$$\frac{\partial \rho}{\partial t} = D\frac{\partial^2 \rho}{\partial x^2}, \tag{2}$$

where $\frac{\partial \rho}{\partial t}$ is the change of alloy element concentration per unit time, $\frac{\partial \rho}{\partial x}$ is the concentration gradient of the alloy element along the diffusion direction $x$, and $D$ is the diffusion coefficient, which is related to alloy elements.

According to Arrhennius equation, the diffusion coefficient $D$ has the following relationship with temperature [26, 27]:

$$D = D_0 \exp\left[-\frac{Q}{RT}\right]. \tag{3}$$

Meanwhile, the analytical formula for the change of mass concentration $\rho$ with distance $x$ and time $t$ is:

$$\rho(x,t) = \frac{\rho_1 + \rho_2}{2} + \frac{\rho_1 - \rho_2}{2}\mathrm{erf}\left(\frac{x}{2\sqrt{Dt}}\right). \tag{4}$$

In Eq. (3), $Q$ is the activation energy of atomic diffusion, $R$ is the gas constant, and $T$ is the temperature.

In Eq. (4), $\rho_1$ and $\rho_2$ is the mass concentration of two substances or two phases that diffuse each other.

It can be seen from Eqs. (2) and (3) that the diffusion coefficient $D$ changes exponentially with the temperature $T$. The change of temperature $T$ leads to the

change of diffusion coefficient $D$ and further leads to the change of $\frac{\partial \rho}{\partial t}$.

The increase of temperature $T$ accelerates the diffusion process of alloy elements and accelerates the rapid progress of $\beta$-phase + AlCu phase $\rightarrow$ I-phase. Therefore, when the heat treatment temperature is 750 ℃, more I-phases are formed than at 650 ℃.

At the same time, the addition of Ce causes component undercooling, and the addition of an appropriate amount of Ce significantly refines the microstructure of the alloy [28, 29]; therefore, when Ce is added to the alloy, the microstructure of the alloy is significantly refined. According to Formula 4, the diffusion time is inversely proportional to the diffusion distance, so the refinement of microstructure reduces the diffusion distance $x$, which significantly shortens the time required for diffusion. Therefore, when the heat treatment temperature is 750 ℃, many quasicrystals can be formed in a short time.

## 4. Conclusions

The microstructure and properties of as-cast and various heat-treated $(Al_{63}Cu_{25}Fe_{12})_{99}Ce_1$ alloy were studied. The results show that:

1. With the increase of heat treatment temperature, the content of the I-phase in $(Al_{63}Cu_{25}Fe_{12})_{99}Ce_1$ alloy increases, and the $\beta$-phase decreases gradually. After $(Al_{63}Cu_{25}Fe_{12})_{99}Ce_1$ alloy was kept at 750 ℃ for 6 h, all $\beta$-phase dissolved and formed almost all I-phase and a small amount of $Al_{13}Ce_2Cu_{13}$ phase.

2. With the increase of heat treatment temperature, the proportion of I-phase first increases to the maximum and then decreases in $(Al_{63}Cu_{25}Fe_{12})_{99}Ce_1$ alloy. After heat treatment at 750 ℃ for 6 h, the proportion of I-phase in the alloy is about 89.116 %, which is 34 % higher than in as-cast alloy.

3. After holding at 750 ℃ for 6 h, $(Al_{63}Cu_{25}Fe_{12})_{99}Ce_1$ alloy has a small thermal expansion coefficient at each temperature stage. Compared with the as-cast alloy, the thermal expansion coefficient of the alloy is reduced by about 10 % at 30–500 ℃.

## Acknowledgements

This study was financially supported by the Shaanxi Creative Talents Promotion Plan-technological Innovation Team under Grant 2017KCT-05; Key Project of Equipment Pre-research Field Fund under Grant 6140922010301; Shaanxi Provincial Key Research and Development Project under Grant 2019ZDLGY05-09; Shaanxi Provincial Education Department to Serve the Local Special Plan Project under Grant 19JC022; and Yulin Science and Technology Bureau Project under Grant 2019-121.

## References

[1] K. Lee, Y. Chen, W. Dai, D. Naugle, H. Liang, Design of quasicrystal alloys with favorable tribological performance in view of microstructure and mechanical properties, Materials & Design 193 (2020) 108735. doi:10.1016/j.matdes.2020.108735

[2] S. M. Lee, B. H. Kim, S. H. Kim, E. Fleury, W. T. Kim, D. H. Kim, Effect of Si addition on the formability of the icosahedral quasicrystalline phase in an Al65Cu20Fe15 alloy, Materials Science and Engineering A 294–296 (2000) 93–98. doi:10.1016/S0921-5093(00)01206-5

[3] E. Karaköse, H. Çolak, Effect of cooling rate and Mg addition on the structural evaluation of rapidly solidified Al-20wt.%Cu-12wt.%Fe alloy, Materials Characterization 121 (2016) 68–75. doi:10.1016/j.matchar.2016.09.030

[4] K. Lee, J. Hsu, D. Naugle, H. Liang, Multi-phase quasicrystalline alloys for superior wear resistance, Materials & Design 108 (2016) 440–447. doi:10.1016/j.matdes.2016.06.113

[5] K. Lee, E. Chen, D. Naugle, H. Liang, Corrosive behavior of multi-phased quasicrystal alloys, Journal of Alloys and Compounds 851 (2021) 156862. doi:10.1016/j.jallcom.2020.156862

[6] A. Tsai, A. Inoue, T. Masumoto, A stable quasicrystal in Al-Cu-Fe system, Japanese Journal of Applied Physics 26 (1987) L1505–L1507. doi:10.1143/jjap.26.l1505

[7] A. P. Tsai, Discovery of stable icosahedral quasicrystals: Progress in understanding structure and properties, Chem. Soc. Rev. 42 (2013) 5352–65. doi:10.1039/c3cs35388e

[8] V. Aghaali, T. Ebadzadeh, Z. Karimi, A. Kazemzadeh, E. Marzbanrad, Effect of mechanical alloying and preheating treatment on the phase transformation of the Al-Cu-Fe compacts annealed by microwave radiation, Journal of Materials Research and Technology 12 (2021) 749–759. doi:10.1016/j.jmrt.2021.02.089

[9] G. Rosas, R. Perez, On the transformations of the $\psi$-AlCuFe icosahedral phase, Materials Letters 47 (2001) 225–230. doi:10.1016/S0167-577X(00)00239-1

[10] H. Parsamehr, C. Yang, W. Liu, S. Chen, S. Chang, L. Chen, A. P. Tsai, C. Lai, Direct observation of growth and stability of Al-Cu-Fe quasicrystal thin films, Acta Materialia 174 (2019) 1–8. doi:10.1016/j.actamat.2019.05.024

[11] W. Wolf, L. P. M. E. Silva, G. Zepon, C. S. Kiminami, C. Bolfarini, W. J. Botta, Single step fabrication by spray forming of large volume Al-based composites reinforced with quasicrystals, Scripta Materialia 181 (2020) 86–91. doi:10.1016/j.scriptamat.2020.02.018

[12] S. M. Lee, H. J. Jeon, B. H. Kim, W. T. Kim, D. H. Kim, Solidification sequence of the icosahedral quasicrystal forming Al-Cu-Fe alloys, Materials Science and Engineering A 304 (2001) 871–878. doi:10.1016/S0921-5093(00)01625-7

[13] F. R. P. Feitosa, R. M. Gomes, M. M. R. Silva, S. J. G. De Lima, J. M. Dubois, Effect of oxygen/fuel ratio on the microstructure and properties of HVOF sprayed Al59Cu25.5Fe12.5B3 quasicrystalline coatings, Surface & Coatings Technology 353 (2018) 171–178. doi:10.1016/j.surfcoat.2018.08.081

[14] W. Steurer, Quasicrystals: What do we know? What do we want to know? What can we know? Acta Crystallographica 74 (2018) 1–11. doi:10.1107/s2053273317016540
[15] L. Zhu, S. Soto-Medina, W. Cuadrado-Castillo, R. G. Hennig, M. V. Manuel, New experimental studies on the phase diagram of the Al-Cu-Fe quasicrystal-forming system, Materials & Design 185 (2020) 108186. doi:10.1016/j.matdes.2019.108186
[16] J. Wang, Z. Ma, H. D. Uan, J. Zhang, D. Tao, J. Li, Effect of the addition of cerium on the microstructure evolution and thermal expansion properties of cast Al-Cu-Fe alloy, Materials Research Express 8 (2021) 036503. doi:10.1088/2053-1591/abe8f4
[17] D. Zhao, R. Wang, J. Wang, W. Qu, N. Shen, J. Gui, The role of the Φ phase in the solidification process of Al-Cu-Fe icosahedral quasicrystal, Materials Letters 57 (2003) 4493–4500. doi:10.1016/S0167-577X(03)00349-5
[18] W. Wolf, C. Bolfarini, C. S. Kiminami, W. J. Botta, Fabrication of Al-matrix composite reinforced with quasicrystals using conventional metallurgical fabrication methods, Scripta Materialia 173 (2019) 21–25. doi:10.1016/j.scriptamat.2019.07.044
[19] H. Parsamehr, T. Chen, D. Wang, M. Leu, I. Han, Z. Xi, A. Tsai, A. J. Shahani, C. Lai, Thermal spray coating of Al-Cu-Fe quasicrystals: Dynamic observations and surface properties, Materialia 8 (2019) 100432. doi:10.1016/j.mtla.2019.100432
[20] L. Zhang, R. Lück, Phase diagram of the Al-Cu-Fe quasicrystal-forming alloy system, Zeitschrift für Metallkunde 94 (2003) 774–781.
[21] L. Zhang, R. Lück, Phase diagram of the Al-Cu-Fe quasicrystal-forming alloy system. II. Isopleths, Zeitschrift für Metallkunde 94 (2003) 98–107.
[22] L. Zhang, R. Lück, Phase diagram of the Al-Cu-Fe quasicrystal-forming alloy system. V. Solidification behaviour of Al-Cu-Fe quasicrystal forming alloys, Zeitschrift für Metallkunde 94 (2003) 774–781.
[23] A. Baker, M. Caputo, H. Hampikian, L. Simpson, C. Li, Icosahedral quasicrystal layer observed on λ phase in Al-Cu-Fe alloy, Materials Sciences and Applications 8 (2017) 509–520. doi:10.4236/msa.2017.87035
[24] A. V. Mikhaylovskaya, A. A. Kishchik, A. D. Kotov, O. V. Rofman, N. Y. Tabachkova, Precipitation behavior and high strain rate superplasticity in a novel fine-grained aluminum based alloy, Materials Science and Engineering A 760 (2019) 37–46. doi:10.1016/j.msea.2019.05.099
[25] H. Zhang, J. Lv, L. Gang, X. Chen, X. Wang, Preparation, characterization, and thermophysical properties of (La0.95Sr0.05)2Ce2O6.95 ceramic for thermal barrier coatings, International Journal of Applied Ceramic Technology 11 (2014) 350–358. doi:10.1111/ijac.12015
[26] G. Hu, X. Cai, and Y. Rong, Fundamentals of Materials Science. Shanghai Jiaotong University Press, 2010.
[27] T. Hong, X. Li, H. Wang, C. Dong, Influence of solution temperature on microstructure and properties of in-situ TiB2/2009 composites, Materials Science & Engineering A 634 (2015) 1–4. doi:10.1016/j.msea.2015.03.037
[28] T. Gong, J. Dong, Z. Shi, X. Yaer, H. Liu, Enhancement of mechanical properties of as-cast 5182 aluminum alloy by Ce-rich modification engineering, Materials Research Express 6 (2019) 086548. doi:10.1088/2053-1591/ab1df7
[29] L. Li, D. Li, F. Mao, J. Feng, Y. Kang, Effect of cooling rate on eutectic Si in Al-7.0Si-0.3Mg alloys modified by La additions, Journal of Alloys and Compounds 826 (2020) 154206. doi:10.1016/j.jallcom.2020.154206